Metastable states and energy flow pathway in square graphene resonators

Yisen Wang,[1] Zhigang Zhu,[1] Yong Zhang,[2] and Liang Huang[1,*]
[1]*School of Physical Science and Technology, and Key Laboratory for Magnetism and Magnetic Materials of MOE, Lanzhou University, Lanzhou, Gansu 730000, China*
[2]*Department of Physics, Xiamen University, Xiamen 361005, China*

(Received 29 October 2017; published 25 January 2018)

Nonlinear interaction between flexural modes is critical to heat conductivity and mechanical vibration of two-dimensional materials such as graphene. Much effort has been devoted to understand the underlying mechanism. In this paper, we examine solely the out-of-plane flexural modes and identify their energy flow pathway during thermalization process. The key is the development of a universal scheme that numerically characterizes the strength of nonlinear interactions between normal modes. In particular, for our square graphene system, the modes are grouped into four classes by their distinct symmetries. The couplings are significantly larger within a class than between classes. As a result, the equations for the normal modes in the same class as the initially excited one can be approximated by driven harmonic oscillators, therefore, they get energy almost instantaneously. Because of the hierarchical organization of the mode coupling, the energy distribution among the modes will arrive at a stable profile, where most of the energy is localized on a few modes, leading to the formation of "natural package" and metastable states. The dynamics for modes in other symmetry classes follows a Mathieu type of equation, thus, interclass energy flow, when the initial excitation energy is small, starts typically when there is a mode that lies in the unstable region in the parameter space of Mathieu equation. Due to strong coupling of the modes inside the class, the whole class will get energy and be lifted up by the unstable mode. This characterizes the energy flow pathway of the system. These results bring fundamental understandings to the Fermi-Pasta-Ulam problem in two-dimensional systems with complex potentials, and reveal clearly the physical picture of dynamical interactions between the flexural modes, which will be crucial to the understanding of their abnormal contribution to heat conduction and nonlinear mechanical vibrations.

DOI: 10.1103/PhysRevE.97.012143

I. INTRODUCTION

Identifying the energy flow pathway has been the core issue of Fermi-Pasta-Ulam (FPU) problem over the past half century. This has been investigated intensively for one-dimensional (1D) nonlinear lattices [1–3]. In particular, for the FPU-β model, the energy flow pathway is obtained analytically based on the sine form of mode functions [4], where the predicted pathway is revealed by numerical calculations correctly. A different approach based on perturbation theory is also proposed [5,6]. Another important issue in FPU problem is that in the small initial energy (or, equivalently, weak nonlinearity) case, there could exist metastable states where the energy can be localized on a small number of modes for extremely long time, hindering equipartition [7,8]. For 1D lattice, metastability is related with Nekhoroshev instability [9], q-breather [10,11], or Toda integrable dynamical behaviors [12,13].

Two-dimensional (2D) materials have attracted much attention due to their peculiar mechanical and transport properties [14–16]. A key feature of 2D materials is that they bear the flexural (out-of-plane) modes, which play an important role in the thermal conductivity [17] and the superior performance of mechanical vibrations [18]. Experimentally, the thermal conductivity of suspended graphene is higher than that of monolayer graphene exfoliated on a substrate because of the strong interface scattering of flexural modes [19]. The relevant numerical calculations also confirm that the flexural phonon modes make a dominated contribution to the thermal conductivity of graphene, which is attributed to the anomalously large density of states of flexural phonons compared to their in-plane counterparts and to a lattice symmetry based selection rule that significantly restricts anharmonic phonon-phonon scattering of the flexural modes [20].

To understand the anharmonic phonon-phonon scattering of the flexural modes, it is critical to treat the nonlinear interaction between these modes. This comes to the Fermi-Pasta-Ulam (FPU) problem [1] naturally, that is, how does the energy initially located at one mode spread to the other modes? For 2D system with only in-plane modes, it has been shown that there are no metastable states [21,22]. For the flexural modes in graphene, it has been found that there exist metastable states in the relaxation process of the fundamental mode, but the microscopic mechanism is unclear [23]. The key problem is thus to reveal the dynamical interaction between the flexural modes and the pathway of the energy flow, to understand the mechanism of the metastable states. While the previous analysis [4–6] of the energy flow pathway can be feasible for 1D lattices and when the nonlinear potential is simple, it is highly nontrivial to extend the method to 2D systems, especially for those with complex potentials such as graphene.

*huangl@lzu.edu.cn

In this paper, we investigate exclusively the metastable states and energy flow pathway between the flexural modes with the nonlinear mode coupling method, which, except heat conduction, is also important for graphene nanomechanical resonators as the out-of-plane motion is their most dominant dynamics [18,24–26]. First, we have developed a numerical procedure, the nonlinear mode coupling method, to characterize the nonlinear interaction between the normal modes, which can be used to calculate the coupling strength between normal modes and determine the pathway of the energy flow during the thermalization process. Second, the application to the energy equipartition among flexural modes in graphene unveils completely the route and microscopic dynamics of thermalization. Interestingly, we have found that the flexural modes are grouped into different classes based on their symmetry properties. The modes within each symmetry class have strong interactions, while the modes belonging to different symmetry classes have much weaker interactions. This hinders energy flow between different symmetry classes. Even within the symmetry class, the strength of the interactions exhibits a hierarchical structure, leading to the formation of metastable states. This confirms the existence of metastable states, and provides a clear physical picture due to the hierarchical organization of nonlinear interactions. For modes in different symmetry classes, the simplified equation is of the Mathieu type, thus, when there is a mode that resides in the unstable region in the parameter space, it will get energy exponentially until its energy is comparable with the initially excited mode. In the meantime, due to the strong couplings of this mode to the other modes in the same symmetry class, the whole class will be lifted up. The system is not equiparticipated, as only these two classes gain energy, while the other symmetry classes still remain small energies. However, when this happens, the coupling matrix **S** will be modified, especially the interclass couplings, which will expedite the equipartition procedure significantly. Our results are of great theoretical significance to help to understand the anharmonic phonon-phonon scattering and the thermalization process of the flexural modes in graphene. Furthermore, because of the symmetry barrier, phonon-phonon scattering between different symmetry classes is significantly suppressed, providing a similar mechanism to reduce the phase space for allowed anharmonic phonon-phonon scattering as observed in [20], contributing to the high thermal conductivity of graphene.

II. MODEL AND MOLECULAR DYNAMICS SIMULATION SETUP

A. Model of the square graphene resonator

We focus on a square graphene resonator with fixed boundaries [Fig. 1(a)], whose interatomic carbon sp^2 bond interactions can be described by the following valence force field (VFF) model [27–30]:

$$U_{sp^2} = \sum_{i=1}^{N} \gamma \mathbf{D}_i \cdot \mathbf{D}_i + \frac{1}{2}\sum_{i=1}^{N}\sum_{j} \frac{\alpha}{4a_0^2}\left(\mathbf{r}_{ij}^2 - a_0^2\right)^2 + \sum_{i=1}^{N}\sum_{j<k} \frac{\beta}{a_0^2}\left(\mathbf{r}_{ij}\cdot\mathbf{r}_{ik} + \frac{1}{2}a_0^2\right)^2, \quad (1)$$

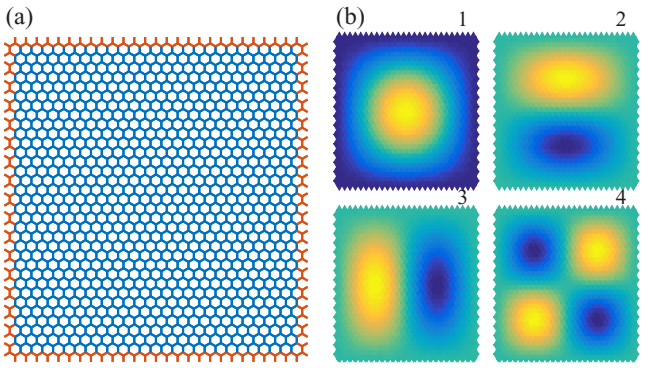

FIG. 1. (a) Setup of the square graphene resonator. The sheet is approximately 6.9 nm by 7.4 nm. It contains 1992 carbon sites in total, the outmost two layers are fixed, and the 1748 inner sites are able to move. (b) The first four normal modes with different symmetries: symmetric-symmetric (SS), antisymmetric-symmetric (AS), SA, and AA along x and y axes. Light gray (yellow) and black (dark blue) indicate maximum and minimum values of the normal modes, respectively.

where N is the system size, i is the site index, j and k are i's nearest neighbors, $\mathbf{r}_{ij}$ is the bond vector from i to j, $a_0 = 1.421$ Å is the equilibrium bond length, $\mathbf{D}_i = \sum_j \mathbf{r}_{ij}$ is the dangling bond vector. The parameters $\alpha = 155.9$ J/m^2, $\beta = 25.5$ J/m^2, and $\gamma = 7.4$ J/m^2 have the same dimension as the coefficient of stiffness [27–30]. The first term of the potential gives the energy cost necessary to change the angle between p_z orbitals, which are approximately normal to the graphene surface. The last two terms represent the energy cost necessary to change the length and angle between covalent C-C bonds.

For the VFF model, the net force acting on site i is determined by the nearest neighbors and the next nearest neighbors of site i. Therefore, the outmost two layers [marked in red in Fig. 1(a)] are fixed during simulations, only the inner sites (blue) can move in the force field according to the Newton's laws of motion.

To address the effect of flexural modes, we consider only the z-direction motion. The VFF model can be simplified as

$$\begin{aligned} U_{sp^2} &= \sum_{i=1}^{N} \gamma \left(\sum_j z_j - 3z_i\right)^2 + \frac{1}{2}\sum_{i=1}^{N}\sum_{j} \frac{\alpha}{4a_0^2}(z_j - z_i)^4 \\ &\quad + \sum_{i=1}^{N}\sum_{j<k} \frac{\beta}{a_0^2}[(z_j - z_i)(z_k - z_i)]^2 \\ &= U^{(2)} + U_1^{(4)} + U_2^{(4)}, \end{aligned} \quad (2)$$

here z_i is the z displacement of site i from its equilibrium position. It is clear that $U^{(2)}$ is the second order potential, which corresponds to the linear interaction, while $U_1^{(4)}$ and $U_2^{(4)}$ are the fourth order potentials. Therefore, the z-direction vibration of graphene system can be effectively an FPU-β model in the hexagonal lattice, which is given by the following potential: $V(x) = x^2 + (\beta'/4)x^4$.

The nonlinearity of the FPU-β model, given by $\beta'\epsilon$, depends on both β' and ϵ, where $\epsilon = E/N$ is the energy per degree of

freedom [13]. The constant β' can be scaled to any positive value by a transformation of variable [31]. In this sense, the ratio of γ to parameters α and β in Eq. (2) does not affect the conclusion of this work. An important parameter for predicting the performance and linearity of graphene nanoelectromechanical devices is the bending rigidity [32] κ, which is related with γ by $\kappa = \sqrt{3}a_0^2\gamma/2$ [30], and in our case, is about 0.8 eV. This value is close to the experimental one (1.2 eV) derived from the phonon spectrum of graphite [33] and falls in the range of 0.5–2.3 eV given by theoretical estimations [34–36]. Based on the above discussions, the specific value of γ and therefore the bending rigidity κ will not affect the qualitative conclusions.

B. General nonlinear mode coupling scheme

In this section, we shall develop a general mode coupling method to analyze the nonlinear interaction between the normal modes. For a lattice such as graphene, the motion equation in real space can be written into the equation of normal coordinates through a mode coupling scheme, as the normal modes form a complete orthonormal basis. The nonlinear mode coupling arises during this procedure due to the existence of the nonlinear term in the potential. By expanding and collecting the nonlinear potentials in terms with the same order of z, we arrive at a neat matrix form for the nonlinear interactions. We shall show that this coupling characterizes the energy flow pathway for this system. This scheme is general and can be applicable for arbitrary lattices with smooth potentials.

In general, for a system with N sites with displacement $\mathbf{z} = [z_1, \ldots, z_N]^T$ and a smooth potential $U(\mathbf{z})$, the potential can be expanded in Taylor series as $U(\mathbf{z}) = U^{(0)} + U^{(1)} + U^{(2)} + \cdots$, where

$$U^{(n)} = \sum_{i_1,\ldots,i_n} \frac{\partial^n U}{\partial z_{i_1} \ldots \partial z_{i_n}}|_{\mathbf{z}=0} z_{i_1} \ldots z_{i_n}$$

is the nth order term. Note that the zeroth order term is a constant that will not yield force and can be set to zero, and the first order term is zero as $\mathbf{z} = 0$ gives the equilibrium position.

The force acting on the ith site is given by $F_i = -\frac{\partial U}{\partial z_i} = \sum_n F_i^{(n)}$, where $F_i^{(n)} = -\frac{\partial U^{(n)}}{\partial z_i}$. Since $U^{(n)}$ is the nth order homogeneous polynomial, $F_i^{(n)}$ can be expressed as

$$F_i^{(n)} = -\frac{1}{n-1} \sum_j \frac{\partial^2 U^{(n)}}{\partial z_i \partial z_j} z_j.$$

Let

$$V_{ij}^{(n)} \equiv -\frac{1}{n-1} \sum_j \frac{\partial^2 U^{(n)}}{\partial z_i \partial z_j},$$

we have $F_i^{(n)} = \sum_j V_{ij}^{(n)} z_j$, and the equation of motion for the ith site is

$$m\ddot{z}_i = F_i = \sum_j V_{ij}^{(2)} z_j + \sum_{n\geqslant 3} \sum_j V_{ij}^{(n)} z_j,$$

or in matrix form for the whole system:

$$m\ddot{\mathbf{z}} = \mathbf{V}^{(2)} \cdot \mathbf{z} + \mathbf{V}^{(\mathrm{nl})} \cdot \mathbf{z}, \tag{3}$$

where $\mathbf{V}^{(2)} = [V_{ij}^{(2)}]_{N\times N}$ and $\mathbf{V}^{(\mathrm{nl})} = [\sum_{n\geqslant 3} V_{ij}^{(n)}]_{N\times N}$ correspond to linear and nonlinear force fields, respectively.

Let $\{\lambda_i, \varphi_i,\ i = 1, \ldots, N\}$ be the set of eigenvalues and eigenvectors of $\mathbf{V}^{(2)}$, i.e., $\mathbf{V}^{(2)}\varphi_i = \lambda_i\varphi_i = -m\omega_i^2\varphi_i$, then φ_i will be the normal mode of the system with eigenfrequency $\omega_i = \sqrt{-\lambda_i/m}$. For a given configuration $\mathbf{z}$ such that $\mathbf{z} = \sum_j c_j\varphi_j$, where c_j are the normal coordinates, denote $\mathbf{c} = [c_1, \ldots, c_N]^T$, Eq. (3) can be written as

$$\sum_j m\ddot{c}_j\varphi_j = \sum_j \mathbf{V}^{(2)} c_j\varphi_j + \sum_j \mathbf{V}^{(\mathrm{nl})} c_j\varphi_j. \tag{4}$$

Left multiplying $\varphi_i^\dagger$ and noting that $\varphi_i^\dagger\varphi_j = \delta_{ij}$, where $\delta_{ij} = 1$ if $i = j$ and zero otherwise, one has

$$m\ddot{c}_i = -m\omega_i^2 c_i + \sum_j S_{ij} c_j, \tag{5}$$

where

$$S_{ij} = \varphi_i^\dagger \mathbf{V}^{(\mathrm{nl})} \varphi_j \tag{6}$$

is the nonlinear mode coupling between mode i and mode j under the nonlinear interaction, whose absolute value can be defined as the coupling strength between the normal modes. Since φ_i is real, we have $S_{ij} = \varphi_i^T \mathbf{V}^{(\mathrm{nl})} \varphi_j$. Denoting $\mathbf{c} = (c_1, \ldots, c_N)^T$, Eq. (5) can be written in the matrix form

$$m\ddot{\mathbf{c}} = \mathbf{\Lambda} \cdot \mathbf{c} + \mathbf{S} \cdot \mathbf{c}, \tag{7}$$

where $\mathbf{\Lambda} = \mathrm{diag}[\lambda_1, \ldots, \lambda_N] = -m\,\mathrm{diag}[\omega_1^2, \ldots, \omega_N^2]$, $\mathbf{S} = [S_{ij}]_{N\times N}$. Typically, $\mathbf{V}^{(\mathrm{nl})}$ depends on the displacements of the sites and is time varying, thus, S_{ij} will also be time dependent, and can actually vary significantly during the evolution. Note that Eqs. (3) and (7) are equivalent, and each provides a complete description to the dynamical evolution of the system.

C. Normal modes for the square graphene resonator

The normal modes $\{\varphi_i,\ i = 1, \ldots, N\}$ for graphene vibration are the eigenvectors of $\mathbf{V}^{(2)}$, which can be derived from the linear term $U^{(2)}$ in the potential. The element of $V^{(2)}$ is given by

$$V_{mn}^{(2)} = \begin{cases} -24\gamma, & n = m \\ 12\gamma, & n = m\text{'s NN} \\ -2\gamma, & n = m\text{'s NNN} \\ 0, & \text{otherwise} \end{cases} \tag{8}$$

where NN denotes nearest neighbors, and NNN denotes next nearest neighbors. For the graphene resonator shown in Fig. 1(a), there are 1748 normal modes in total, which is equal to the number of movable sites.

Due to mirror symmetry of the quadratic potential of the system, the normal modes are either symmetric (S) or antisymmetric (A) with respect to the x or y axes, and are grouped into four different classes: SS, SA, AS, and AA. Figure 1(b) shows the first four normal modes, which belong to these four symmetry classes, respectively. In addition, we have also derived the dispersion relation from the linear potential $U^{(2)}$ of the VFF model, which is consistent with previous results [29]. The minimum and maximum eigenfrequencies from $\mathbf{V}^{(2)}$ of the graphene resonator are 3.04×10^{11} rad/s (48.4 GHz) and 1.63×10^{14} rad/s (26.0 THz), respectively.

To characterize the relative magnitude of the linear and nonlinear potentials, we deform the graphene sheet according

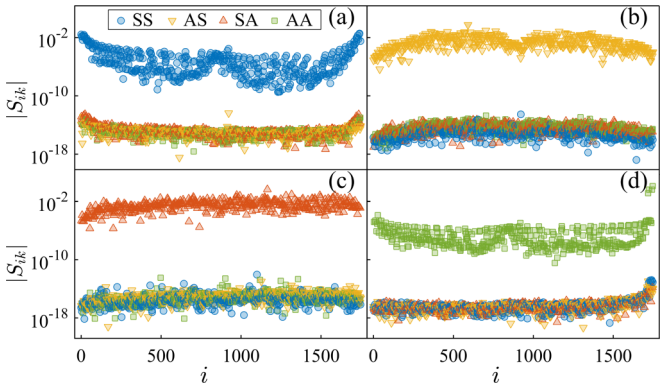

FIG. 2. The coupling strength $|S_{ik}|$ between the initially excited mode k and the other modes. The initially excited modes are 1, 592, 1165, and 1746 for (a)–(d), belonging to the four different symmetry classes, respectively. The corresponding specific energies [Eq. (2)] are $\epsilon = 1.7524 \times 10^{-22}$ J, 2.1343×10^{-22} J, 1.2134×10^{-22} J, and 3.3978×10^{-22} J. The system is 6.9 nm by 7.2 nm (1748 movable sites). The first half modes, say $i \leqslant 874$, are in acoustical branch. The last half modes ($i > 874$) are in optical branch. The four symmetry classes are marked by different symbols, as shown in (a).

to the first normal mode, $z_i \sim \varphi_{1,i}$, and calculate the linear potential $U^{(2)}$ and the nonlinear potentials $U_1^{(4)}$ and $U_2^{(4)}$. It is found that they have a cross point at specific energy $\epsilon \sim 10^{-23}$ J per each site. Thus, if the specific energy is smaller than this value, the linear potential dominates; while if the energy is large, then the nonlinear potential dominates.

D. Symmetry classes of the modes

In order to determine the nonlinear interaction between flexural modes, the graphene sheet is deformed by assigning an out-of-plane displacement profile corresponding to a particular normal mode. The total energy can then be calculated with Eq. (2), and the nonlinear coupling is calculated with Eq. (6). Figure 2 shows the coupling strength between the initially excited flexural mode and all the other modes. Modes in different symmetry classes are plotted with different colors and symbols. It is clear that, for a given initially excited mode, only the couplings with modes belonging to the same symmetry class are significant, while the values for the other modes are about 10 orders smaller, which can be neglected in the beginning of the equipartition process. This forms the blockade that hinders energy flow between different symmetry classes. Thus, the coupling between the modes is mainly determined by the symmetry class. This has been noticed in the original FPU paper [1] that when a symmetric quartic potential is applied and the lattice is initially perturbed using an odd mode, the symmetry will be kept and only a few odd modes can be excited. Note that there are some interclass couplings that are also discernible, such as the coupling strength between mode 1 and the first few modes in the SA class as shown in Fig. 2(a). These couplings play a key role in the process of equipartition by breaking the barrier and guiding energy flow between different symmetry classes.

Previous observations show that when the initial excitation is on the lower modes, typically only modes close to the initially excited mode will gain energy, and the energy gaining rate decreases fast as it goes away from that mode [7,10,37]. As shown in Fig. 2(a), this is the case if we only consider the modes in the same symmetry class. Even though, it is not monotonic, as it goes up in the end of the optical branch. While for other cases [Figs. 2(b)–2(d)], this feature is absent, where long range correlations are dominant. Another feature is that the acoustical branch and the optical branch are densely correlated. For any given initial excitation, its couplings to the modes in the acoustical branch and modes in the optical branch are in the same range.

In addition, Fig. 2 indicates that there are fine, hierarchical structures of the nonlinear couplings in the same symmetry class, where the variations change systematically when the mode number changes. This plays an important role in the formation of metastable states.

E. Setup for molecular dynamics simulation

In our simulations, the graphene sheet is initially deformed in the z direction proportional to a particular normal mode. The ineluctable thermal motion and thermal random forces existing in real systems will expedite the thermalization process. To better understand the role of dynamics of this initial thermalization and equipartition process as in the FPU problem, the thermal motion and thermal random forces are neglected during our simulation and the initial velocities are set to zero.

The molecular dynamics (MD) simulations are performed using the potential in Eq. (2), where the verlet algorithm is used for integration with a time step of 0.5 fs. When $\mathbf{z}(\mathbf{t})$ is solved, it can be projected to the normal modes to get the normal coordinates $\langle \varphi_j | \mathbf{z} \rangle = c_j$ or $\mathbf{z} = \sum_j c_j \varphi_j$ and the harmonic energy, i.e., the quadratic part of the energy of mode i is given by [38,39]

$$E_i(t) = \tfrac{1}{2} m \left(\dot{c_i}^2 + \omega_i^2 c_i^2 \right). \tag{9}$$

III. ENERGY FLOW PATHWAY

The route to energy equipartition is mostly determined by the coupling matrix $\mathbf{S}$. Based on the symmetry properties of the normal modes, they are grouped into four different symmetry classes. The couplings (nonlinear interaction caused by the nonlinear potentials) between modes in the same class are dominantly larger than those between modes belonging to different classes. This hinders energy flow between different classes. As a result, the modes in the same class as the initially excited mode follow the driven harmonic oscillator equation, and get energy instantaneously. To break the blockade, for modes in other symmetry classes and when the initial excitation energy is small, the normal coordinates follow the Mathieu type of equation. Thus, if there exists one mode that resides in the unstable region in the parameter space, this mode will get energy exponentially, and lift up the whole symmetry class that it belongs to through the strong couplings. If none of the modes reside in the unstable region, then they will remain at small energies for a substantially long time. Due to the hierarchical organization of the nonlinear couplings within a symmetry class, when the energy is small, a natural packet is formed and results in metastable states. The detailed analysis is provided as follows.

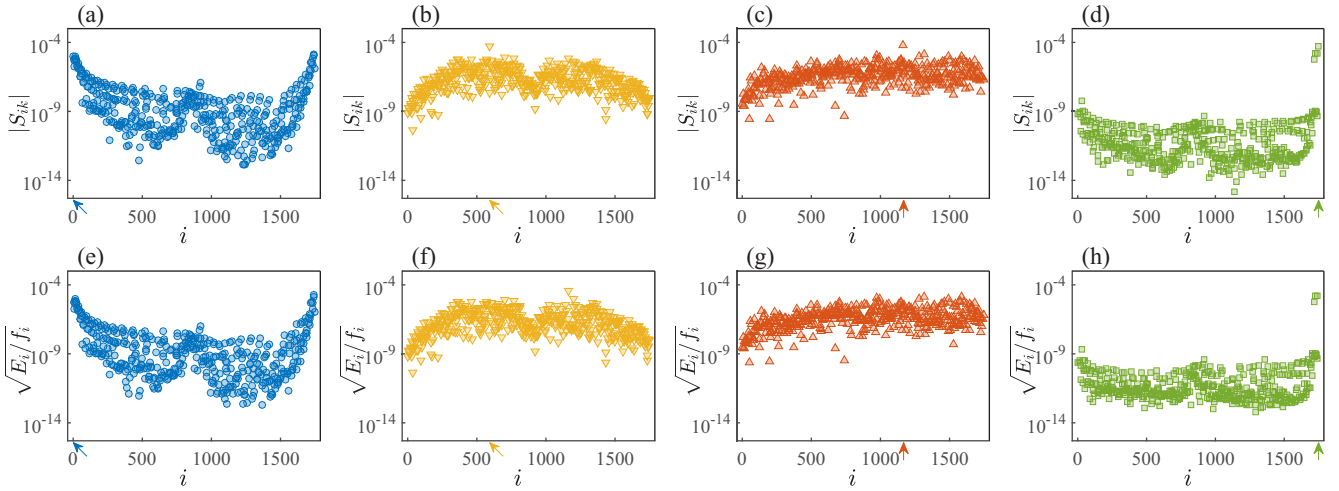

FIG. 3. (a)–(d) The nonlinear mode coupling $|S_{ik}|$ between the initially excited mode k and the other modes. The initially excited mode k is 1, 592, 1165, and 1746 for (a)–(d), which belong to four different symmetry classes, respectively. The symbols are the same as Fig. 2, but only the modes in the same symmetry class are plotted. The corresponding excitation specific energies are smaller than that in Fig. 2, i.e., $\epsilon = 7.8919 \times 10^{-27}$, 2.1240×10^{-26}, 1.8944×10^{-26}, and 1.5085×10^{-26} J. (e)–(h) The plots of $\sqrt{E_i(t)/f_i(t)}$ versus i except mode k for the same initial excitations as (a)–(d), respectively, at $t = 12$ ps.

Starting from Eq. (7), if only one mode is excited in the beginning, say, the kth mode, then in the initial steps, only c_k has a finite value, while all other normal coordinates have vanishing values. Therefore, the interactions between these modes are negligible, and they can be regarded as driven systems where the driving forces come from the kth mode:

$$m\ddot{\mathbf{c}} \approx \Lambda \cdot \mathbf{c} + \mathrm{diag}(\mathbf{S}) \cdot \mathbf{c} + \mathbf{S}_k c_k, \tag{10}$$

where $\mathbf{S}_k$ is the kth column of matrix $\mathbf{S}$. The second term on the right-hand side (RHS) is nonlinear self-interaction, it is kept as it can be important in certain cases. For a mode i that is different from k, it becomes

$$m\ddot{c}_i \approx -m\omega_i^2 c_i + S_{ii} c_i + S_{ik} c_k. \tag{11}$$

A. Dynamics of modes in the same symmetry class

For modes belonging to the same symmetry class as the initially excited mode k, since $|S_{ik}|$ is large (Fig. 2), when $|c_i| \ll |c_k|$, the second term on the RHS of Eq. (11) can be neglected, and we get an analytically solvable model, the driven harmonic oscillator:

$$m\ddot{c}_i \approx -m\omega_i^2 c_i + S_{ik} c_k. \tag{12}$$

Note that $c_k(t) \approx \widetilde{C}\cos(\omega_k t)$ and $S_{ik}(t) \approx S_{ik}(0)\cos^2(\omega_k t)$, thus,

$$m\ddot{c}_i \approx -m\omega_i^2 c_i + S_{ik}(0)\widetilde{C}\cos^3(\omega_k t), \tag{13}$$

which is a forced harmonic oscillator. The analytical solution is

$$c_i(t) = \left[3\left(\omega_i^2 - 9\omega_k^2\right)\cos(\omega_k t) + \left(\omega_i^2 - \omega_k^2\right)\cos(3\omega_k t) + 4\left(7\omega_k^2 - \omega_i^2\right)\cos(\omega_i t)\right] \Big/ \left[4m\left(9\omega_k^4 - 10\omega_k^2\omega_i^2 + \omega_i^4\right)\right] \times \widetilde{C} S_{ik}(0), \tag{14}$$

the corresponding velocity is

$$\dot{c}_i(t) = -\left[3\left(\omega_i^2 - 9\omega_k^2\right)\omega_k \sin(\omega_k t) + 3\left(\omega_i^2 - \omega_k^2\right)\omega_k \sin(3\omega_k t) + 4\left(7\omega_k^2 - \omega_i^2\right)\omega_i \sin(\omega_i t)\right] \Big/ \left[4m\left(9\omega_k^4 - 10\omega_k^2\omega_i^2 + \omega_i^4\right)\right] \times \widetilde{C} S_{ik}(0). \tag{15}$$

The instantaneous energy of mode i is given by

$$E_i(t) = \tfrac{1}{2}m\left[\dot{c}_i{}^2(t) + \omega_i^2 c_i^2(t)\right] \propto S_{ik}^2(0). \tag{16}$$

The time varying part of $E_i(t)$ can be denoted as $f_i(t)$, thus, $E_i(t) = f_i(t)S_{ik}^2(0)$. Therefore, for a given initial excitation on mode k, in the beginning of the evolution, the energy of the modes is solely determined by the nonlinear mode coupling S_{ik} evaluated at the $t = 0$. Thus, S_{ik} determines the energy flow from the initial excited mode k to the other modes. On the other hand, if one gets $E_i(t)$ from simulation, then one can infer $S_{ik}(0)$, i.e., by $\sqrt{E_i(t)/f_i(t)}$.

Figures 3(a)–3(d) show the nonlinear mode coupling strength $|S_{ik}(0)|$ for four modes belonging to different symmetry classes. In order to check the validity of the solution (16), the MD simulations are performed for the same initial excitations as in Figs. 3(a)–3(d), and the energy spectrum $E_i(t)$ is obtained. Figures 3(e)–3(h) plot $\sqrt{E_i(t)/f_i(t)}$ versus i at $t = 12$ ps (24 000 time steps). It is clear that for all the four cases $\sqrt{E_i(t)/f_i(t)}$ recover the nonlinear mode coupling $|S_{ik}(0)|$ exactly. Note that, the dynamics of the modes in the same symmetry class, given by Eq. (13), is not resonant and only involves the coupling between the mode i and the initially excited mode k, which behaves as a driven harmonic oscillator. This equation is only valid at the beginning of the simulation when the initial excited energy is small. When the initial excited energy increases or the time is large, the coupling between the modes other than the initially excited one will become large, which will result in the energy flow between them.

Figure 4 compares the energy spectra for full molecular dynamics simulation [Eq. (3), Figs. 4(a) and 4(e)], the full

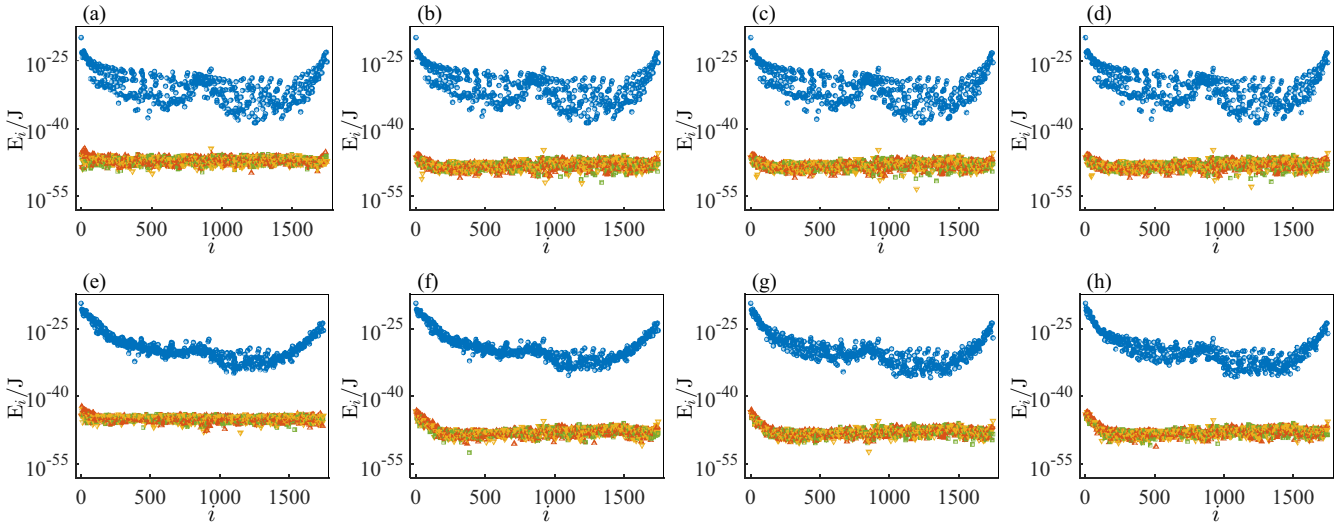

FIG. 4. Comparison of the energy spectra obtained from full molecular dynamics simulation [Eq. (3), panels (a) and (e)], the full mode coupling dynamics simulation [Eq. (7), panels (b) and (f)], the simplified version of the mode coupling dynamics simulation [Eq. (10), panels (c) and (g)], and the further simplified version of the mode coupling dynamics simulation [Eq. (13), panels (d) and (h)]. The excitation is on the first mode. The initial energy is 2.7242×10^{-23} J. The upper panels are for $t = 0.027$ ps, and the lower panels are for $t = 23.995$ ps.

mode coupling dynamics simulation [Eq. (7), Figs. 4(b) and 4(f)], the simplified version [Eq. (10), Figs. 4(c) and 4(g)], and the further simplified version [Eq. (13), Figs. 4(d) and 4(h)]. One can see that the energies, especially those for the first symmetry class, are the same for the full molecular dynamics simulation and the full mode coupling dynamics simulation, e.g., Fig. 4(a) versus 4(b) and Fig. 4(e) versus 4(f). For the simplified version, when t is small [Figs. 4(c) and 4(d)], it is identical to the full version. For longer time [Figs. 4(g) and 4(h)] there appear discrepancies comparing with the full simulation [Figs. 4(e) and 4(f)], but the main structures both inside cluster and between clusters are kept. The discrepancy between Figs. 4(f) and 4(g) comes from the neglect of the couplings between the modes other than the initially excited one in Fig. 4(g). As a result, the energy flow between these modes is neglected, and their energies have a larger span than those in Fig. 4(f). In other words, the energy is more uniform in Fig. 4(f) than in Fig. 4(g). Figures 4(g) and 4(h) are almost identical to each other. This implies that the further simplification of removing the nonlinear self-interaction term has no effects to the dynamical evolution of the modes.

B. Dynamics of modes in different symmetry classes

For dynamics of modes in different symmetry classes, since $|S_{ik}|$ is small (Fig. 2), the second term on the RHS of Eq. (11) is also important. To proceed, a detailed expression of S_{ij} is required. In particular, if the nonlinear terms are of the same order, say, $U^{(4)}$, as in our graphene resonator case, then

$$V_{pq}{}^{(4)} = -\frac{1}{3}\frac{\partial^2 U^{(4)}}{\partial z_p \partial z_q} = \sum_{m,n} C_{pqmn} z_m z_n, \tag{17}$$

where C_{pqmn} are the coefficients and can be determined from the expression of $U^{(4)}$. According to $\mathbf{z} = \sum_r c_r \varphi_r$, the mth element of $\mathbf{z}$ can be written as $z_m = \sum_r c_r \varphi_{r,m}$, where $\varphi_{r,m}$ is the mth element of φ_r. Thus, we have

$$V_{pq}^{(4)} = \sum_{m,n,r,s} C_{pqmn} \varphi_{r,m} \varphi_{s,n} c_r c_s. \tag{18}$$

As a result, the mode coupling between the jth normal mode and ith normal mode can be written as

$$S_{ij} = \sum_{p,q} \varphi_{i,p} V_{pq}^{(4)} \varphi_{j,q}. \tag{19}$$

Substituting Eq. (18) into Eq. (19), we have

$$\begin{aligned} S_{ij} &= \sum_{p,q,m,n,r,s} C_{pqmn} \varphi_{i,p} \varphi_{r,m} \varphi_{s,n} \varphi_{j,q} c_r c_s \\ &= \sum_{r,s} W_{ij,rs} c_r c_s, \end{aligned} \tag{20}$$

where

$$W_{ij,rs} = \sum_{p,q,m,n} C_{pqmn} \varphi_{i,p} \varphi_{r,m} \varphi_{s,n} \varphi_{j,q}. \tag{21}$$

Note that the above expansion for S_{ij} is advantageous only for analytical analysis, numerically it will require too much computation power for summation over the six indices, e.g., $\sim N^6$ calculations for each S_{ij}, and $\sim N^8$ calculations for the whole $\mathbf{S}$ matrix. This renders the expansion useless for large systems. The numerical method that calculates $S_{ij} = \varphi_i^T \mathbf{V}^{(\mathrm{nl})} \varphi_j$ directly is more efficient once $\mathbf{V}^{(\mathrm{nl})}$ is obtained.

The two terms on the RHS of Eq. (11), neglecting the influence from other modes, can be written as

$$\begin{aligned} S_{ii} c_i &= \sum_{r,s} W_{ii,rs} c_r c_s c_i \simeq W_{ii,kk} c_k^2 c_i + W_{ii,ki} c_k c_i^2 \\ &\quad + W_{ii,ik} c_k c_i^2 + W_{ii,ii} c_i^3, \\ S_{ik} c_k &= \sum_{r,s} W_{ik,rs} c_r c_s c_k \simeq W_{ik,kk} c_k^3 + W_{ik,ki} c_k^2 c_i \\ &\quad + W_{ik,ik} c_k^2 c_i + W_{ik,ii} c_k c_i^2. \end{aligned} \tag{22}$$

Substituting Eq. (22) into Eq. (11), the motion equation of c_i can be written as

$$m\ddot{c}_i = -m\omega_i^2 c_i + S_1 c_k^2 c_i + S_2 c_k c_i^2 + S_3 c_i^3 + S_k c_k^3, \quad (23)$$

where

$$\begin{aligned} S_1 &= W_{ii,kk} + W_{ik,ki} + W_{ik,ik}, \\ S_2 &= W_{ii,ki} + W_{ii,ik} + W_{ik,ii}, \\ S_3 &= W_{ii,ii}, \quad S_k = W_{ik,kk} \end{aligned} \quad (24)$$

are constants. When the initial excitation energy is small, c_k can be approximated as $c_k(t) \approx c_k(0)\cos(\omega_k t)$. Note that when $|c_i| \ll |c_k|$, collecting the terms based on the orders of c_k in Eq. (22) and keeping only the highest order term of c_k, one has only $S_k c_k^3$, thus $S_k c_k^3 \approx S_{ik} c_k$, returning to Eq. (12).

Let

$$\begin{aligned} \tilde{t} &= \omega_k t, \quad Q_i = \frac{S_1 c_k(0)^2}{4m\omega_k^2}, \\ A_i &= \frac{1}{\omega_k^2}\left[\omega_i^2 - \frac{S_1 c_k(0)^2}{2m}\right], \\ g_i(\tilde{t}) &= \frac{1}{m\omega_k^2}(S_2 c_k c_i^2 + S_3 c_i^3 + S_k c_k^3), \end{aligned} \quad (25)$$

Eq. (23) becomes

$$\frac{d^2 c_i}{d\tilde{t}^2} + [A_i - 2Q_i\cos(2\tilde{t})]c_i = g_i(\tilde{t}). \quad (26)$$

If $g_i(\tilde{t}) = 0$, then it becomes the Mathieu equation

$$\frac{d^2 c_i}{d\tilde{t}^2} + [A_i - 2Q_i\cos(2\tilde{t})]c_i = 0, \quad (27)$$

which describes the phenomena of parametric resonance. In particular, depending on the values of Q_i and A_i, the parameter space (Q_i, A_i) is divided into stable region and unstable region. When the parameters (Q_i, A_i) reside in the unstable region, which originates from $(Q_i, A_i) = (0, n^2)$, where n is an integer, c_i diverges exponentially [40]. For nonzero but small $g_i(\tilde{t})$, the boundary of the unstable region is basically the same [4]. The nonlinear terms of c_i in $g_i(\tilde{t})$ balance the divergence when c_i is large, keeping c_i a finite value [41,42]. The term $S_k c_k^3$ in $g_i(\tilde{t})$ introduces driving from mode k. The key parameters (Q_i, A_i) depend on the initial excitation energy through $c_k(0)$. In general, when the initial excitation goes to zero, $Q_i \to 0$ and $A_i \to (\omega_i/\omega_k)^2$. As the initial excitation energy becomes larger, Q_i increases and A_i decreases. Therefore, for a given k, if there exists some mode i such that ω_i/ω_k is a little bit larger than an integer n, then as the initial excitation energy increases, since Q_i increases and A_i decreases, it will intersect with the unstable region originated from $(Q_i, A_i) = (0, n^2)$. When this happens, this mode will gain energy exponentially until its energy reaches comparable value close to E_k. In the meantime, because the strong couplings between this mode and other modes in the same symmetry class, the whole class will be lifted up, expediting energy equipartition.

Figure 5(a) shows the unstable region for the Mathieu equation. In the case when the first mode is excited initially with specific energy $\epsilon = 1.1148 \times 10^{-24}$ J, we have calculated (Q_i, A_i) for the first four modes, and plotted in Fig. 5(a) as crosses. It is found that (Q_3, A_3) resides in the unstable region, thus,

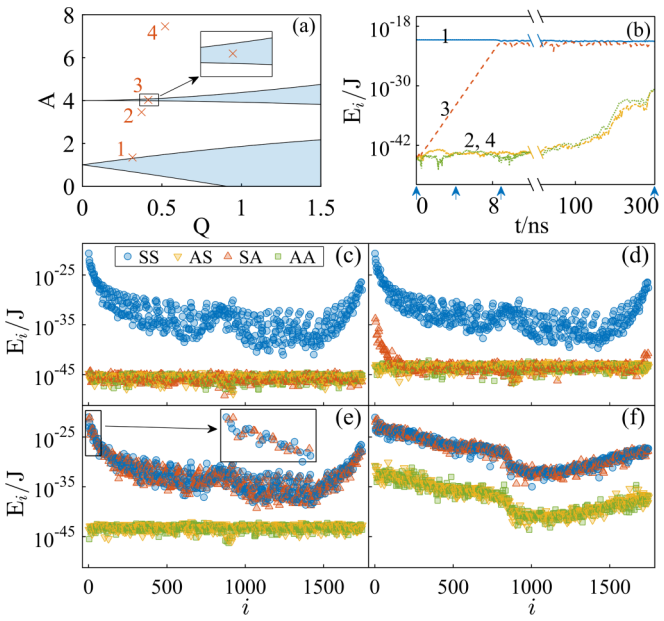

FIG. 5. (a) The stable (white) and unstable (blue or gray) regions of Mathieu equation. Initially, mode 1 is excited with specific energy $\epsilon = 1.1148 \times 10^{-24}$ J. The crosses mark the parameters (Q_i, A_i) calculated from Eqs. (24) and (25) for the first four modes. (b) The time evolution of the harmonic energy for the first four modes. (c)–(f) The energy spectrum at different time instances as marked by blue arrows in (b), the corresponding time is 0.02, 4.18, 8.90, and 300 ns, respectively. Inset of (e): zoom-in of the energy spectrum for the lower modes.

mode 3 (Q_3, A_3) is unstable. Figure 5(b) plots the harmonic energy for the first four modes from the MD simulation. The energy of mode 3 increases exponentially. At around $t = 9$ ns, the energy of mode 3 becomes comparable to mode 1, the initially excited mode. In the meantime, the energies of modes 2 and 4 are basically unchanged. Note that as mode 3 gains energy, the whole class that has the same symmetry is lifted up through couplings with mode 3 [Figs. 5(d) and 5(e)]. At this time, the energy of the modes close to mode 1 decreases exponentially as the mode number increases, which can be regarded as a "natural package" [Fig. 5(e)]. However, this "package" is not stable, as the excitation of the two different classes of modes changes the coupling matrix **S** substantially, especially the interclass couplings, which expedites the energy equipartition process. As Fig. 5(b) shows, for a longer time, when $t > 100$ ns, the energy of modes 2 and 4 also increases gradually. This can be seen in Fig. 5(f), that not only classes 2 and 4 gain energy, but the fine structure in classes 1 and 3 is also diminished. Modes in classes 2 and 4 will gain energy gradually, keeping the energy spectrum in the same profile, until arrive comparable energy with the classes 1 and 3. This profile with different behaviors in the acoustic branch and the optical branch will become flattened afterwards, reaching equipartition. The procedure from Fig. 5(f) to equipartition is the same as the cases with a much larger initial energy, but is much slower, or with a much larger time scale.

However, when the initial energy is a little bit larger (1.4428×10^{-24} J), mode 3 moves out of the unstable region, and none of the modes except those in class 1 gain energy,

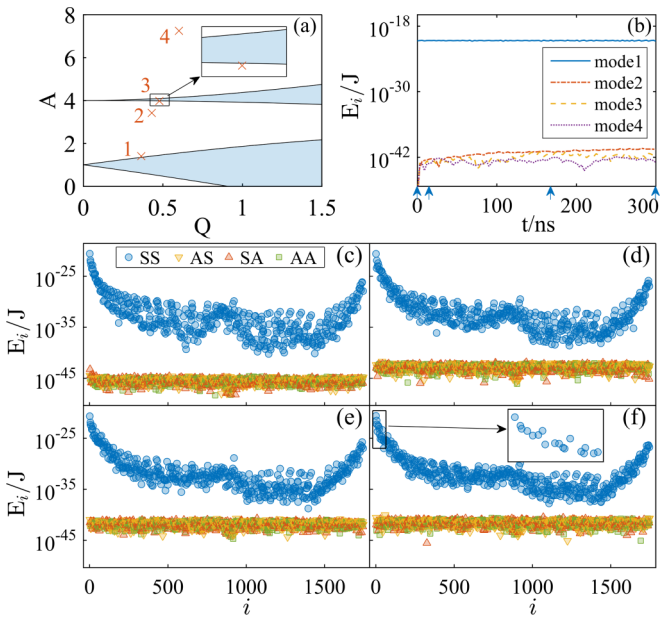

FIG. 6. The same plots as Fig. 5 except that the initial excitation energy is a little bit larger: $\epsilon = 1.4428 \times 10^{-24}$ J. The time instances for the energy spectrum (c)–(f) are 0.03, 14.97, 167.90, and 300 ns, respectively. Inset of (f): zoom-in of the energy spectrum for the lower modes.

as shown in Fig. 6. Furthermore, the energies for the first few modes in class 1 decrease exponentially as the mode number increases, as shown in Fig. 6(f). Note that the plot is in logarithmic scale, thus, the first few modes occupy most of the energy of the system, leading to the formation of "natural packets," where a few modes gain energy quickly and form a stable combination in a substantially long period [8]. This provides concrete evidence for the metastability when the energy is small, that the system can be stable for an extremely long period, e.g., 300 ns, before equipartition might occur.

IV. DISCUSSIONS AND CONCLUSION

To conclude, we have developed a numerical procedure to characterize the nonlinear interaction between the normal modes. Based on this method, the coupling strength between normal modes can be estimated, which can predict the formation of "natural packets" in the normal coordinates' profile, and determine the pathway of the energy flow during the thermalization process. Note that our method is general and is applicable to arbitrary nonlinear lattices with smooth potentials.

For the graphene lattice, the flexural modes are divided into different classes owing to their symmetries, where intraclass interactions are significantly stronger than interclass interactions. Therefore, in the case of small initial excitation energy, only the modes belonging to the same class can be excited, forming a natural packet based on the hierarchical structure in S_{ik}, leading to metastable states. Interclass barrier can be broken if there is a mode that falls in the Mathieu instability region, that it gains energy exponentially with time, lifting the whole class of modes with the same symmetry. Although a natural packet seems to form in the beginning, S_{ij} could change substantially during the evolution. As a result, the modes in the other symmetry classes will also gain energy, leading to expedited equipartition.

Note that the above picture about energy flow pathway is general, as our analysis, e.g., Eqs. (10)–(27), are independent to the particular mode that is initially excited. For different initial modes, the energy flow rates and the detailed pathways should be different, but the phenomena are qualitatively the same. These results reveal the dynamical organization and the route to equipartition of the flexural modes, which are crucial to the understandings of thermalization of the flexural modes and their peculiar contributions to the high heat conductivity and nonlinear vibrations.

ACKNOWLEDGMENTS

We thank Prof. H. Zhao, Prof. L. Rondoni, and Prof. G. Casati for illuminating discussions. This work was supported by NNSF of China under Grants No. 11335006, No. 11375074, No. 11422541, and 11775101, by President Foundation of Xiamen University under Grant No. 20720150036, and by the Fundamental Research Funds for the Central Universities under Grant No. lzujbky-2016-k05.

APPENDIX: FORCE FIELD FOR THE NONLINEAR POTENTIALS

The force fields $\mathbf{V}_1^{(4)}$ and $\mathbf{V}_2^{(4)}$ for the nonlinear potentials $U_1^{(4)}$ and $U_2^{(4)}$ can be derived as

$$V_{1,mn}^{(4)} = \begin{cases} -\sum_{j=m\text{'s NN}} \frac{\alpha}{a_0^2}(z_j - z_m)^2, & n = m \\ \frac{\alpha}{a_0^2}(z_n - z_m)^2, & n = m\text{'s NN} \\ 0, & \text{otherwise} \end{cases}$$

and

$$V_{2,mn}^{(4)} = \begin{cases} -\sum_{\substack{j,k=m\text{'s NN} \\ j\neq k}} \frac{2\beta}{3a_0^2}[(z_k - z_m)(2z_j + z_k - 3z_m) + (z_j - z_m)(2z_k + z_j - 3z_m)] \\ -\sum_{j=m\text{'s NN}} \sum_{\substack{l=j\text{'s NN} \\ l\neq m}} \frac{2\beta}{3a_0^2}(z_l - z_j)^2, & n = m \\ -\sum_{\substack{k=m\text{'s NN} \\ k\neq n}} \frac{2\beta}{3a_0^2}[(z_k - z_m)(3z_m - 2z_n - z_k)] \\ +\sum_{\substack{l=n\text{'s NN} \\ l\neq m}} \frac{2\beta}{3a_0^2}[(z_l - z_n)(z_l + 2z_m - 3z_n)], & n = m\text{'s NN} \\ -\frac{4\beta}{3a_0^2}(z_m - z_j)(z_n - z_j), & n = m\text{'s NNN, } j = m \text{ and } n\text{'s NN} \\ 0, & \text{otherwise.} \end{cases}$$

[1] E. Fermi, J. Pasta, and S. Ulam, Studies of Nonlinear Problems, Tech. Rep. (Los Alamos Scientific Laboratory Report No. LA-1940) (unpublished); in *Collected Papers of Enrico Fermi*, edited by E. Segr (University of Chicago Press, Chicago, 1965), Vol. 2, p. 978 (1955).

[2] F. M. Izrailev and B. V. Chirikov, Dokl. Akad. Nauk SSSR **166**, 57 (1966) [Sov. Phys. Dokl **11**, 30 (1966)].

[3] F. M. Izrailev, A. I. Khisamutdinov, and B. V. Chirikov, Report 252, Institute of Nuclear Physics, Novosibirsk, USSR, 1968 (English translation: LA-4440-TR, Los Alamos, 1970).

[4] N. Sait, N. Hirotomi, and A. Ichimura, J. Phys. Soc. Jpn. **39**, 1431 (1975).

[5] D. S. Sholl and B. I. Henry, Phys. Lett. A **159**, 21 (1991).

[6] D. S. Sholl and B. I. Henry, Phys. Rev. A **44**, 6364 (1991).

[7] F. Fucito, F. Marchesoni, E. Marinari, G. Parisi, L. Peliti, S. Ruffo, and A. Vulpiani, J. Phys. (Paris) **43**, 707 (1982).

[8] L. Berchialla, L. Galgani, and A. Giorgilli, Discrete Contin. Dyn. Syst. **11**, 855 (2004).

[9] M. Pettini and M. Landolfi, Phys. Rev. A **41**, 768 (1990).

[10] S. Flach, M. V. Ivanchenko, and O. I. Kanakov, Phys. Rev. Lett. **95**, 064102 (2005).

[11] S. Flach, M. V. Ivanchenko, and O. I. Kanakov, Phys. Rev. E **73**, 036618 (2006).

[12] M. Toda, Prog. Theor. Phys. Suppl. **45**, 174 (1970).

[13] G. Benettin, H. Christodoulidi, and A. Ponno, J. Stat. Phys. **152**, 195 (2013).

[14] C. Lee, X. Wei, J. W. Kysar, and J. Hone, Science **321**, 385 (2008).

[15] S. D. Sarma, S. Adam, E. Hwang, and E. Rossi, Rev. Mod. Phys. **83**, 407 (2011).

[16] A. A. Balandin, Nat. Mater. **10**, 569 (2011).

[17] E. Pop, V. Varshney, and A. K. Roy, MRS Bull. **37**, 1273 (2012).

[18] J. S. Bunch, A. M. van der Zande, S. S. Verbridge, I. W. Frank, D. M. Tanenbaum, J. M. Parpia, H. G. Craighead, and P. L. McEuen, Science **315**, 490 (2007).

[19] J. H. Seol, I. Jo, A. L. Moore, L. Lindsay, Z. H. Aitken, M. T. Pettes, X. Li, Z. Yao, R. Huang, D. Broido *et al.*, Science **328**, 213 (2010).

[20] L. Lindsay, D. A. Broido, and N. Mingo, Phys. Rev. B **82**, 115427 (2010).

[21] G. Benettin, Chaos **15**, 015108 (2005).

[22] G. Benettin and G. Gradenigo, Chaos **18**, 013112 (2008).

[23] D. Midtvedt, A. Croy, A. Isacsson, Z. Qi, and H. S. Park, Phys. Rev. Lett. **112**, 145503 (2014).

[24] R. A. Barton, B. Ilic, A. M. van der Zande, W. S. Whitney, P. L. McEuen, J. M. Parpia, and H. G. Craighead, Nano Lett. **11**, 1232 (2011).

[25] C. Chen, S. Rosenblatt, K. I. Bolotin, W. Kalb, P. Kim, I. Kymissis, H. L. Stormer, T. F. Heinz, and J. Hone, Nat. Nanotechnol. **4**, 861 (2009).

[26] A. Eichler, J. Moser, J. Chaste, M. Zdrojek, I. Wilson-Rae, and A. Bachtold, Nat. Nanotechnol. **6**, 339 (2011).

[27] P. N. Keating, Phys. Rev. **145**, 637 (1966).

[28] R. M. Martin, Phys. Rev. B **1**, 4005 (1970).

[29] C. Lobo and J. Łułs, Z. Phys. D **39**, 159 (1997).

[30] J. M. K. J. Atalaya and A. Isacsson, Nano Lett. **8**, 4196 (2008).

[31] J. De Luca, A. J. Lichtenberg, and S. Ruffo, Phys. Rev. E **60**, 3781 (1999).

[32] N. Lindahl, D. Midtvedt, J. Svensson, O. A. Nerushev, N. Lindvall, A. Isacsson, and E. E. B. Campbell, Nano Lett. **12**, 3526 (2012).

[33] R. Nicklow, N. Wakabayashi, and H. G. Smith, Phys. Rev. B **5**, 4951 (1972).

[34] W. H. Duan and C. M. Wang, Nanotechnology **20**, 075702 (2009).

[35] D.-B. Zhang, E. Akatyeva, and T. Dumitrică, Phys. Rev. Lett. **106**, 255503 (2011).

[36] J. W. Kang and S. Lee, Comput. Mater. Sci. **74**, 107 (2013).

[37] T. Penati and S. Flach, Chaos **17**, 023102 (2007).

[38] G. Berman and F. Izrailev, Chaos **15**, 015104 (2005).

[39] H. J. Matsuyama and T. Konishi, Phys. Rev. E **92**, 022917 (2015).

[40] N. W. McLachlan, *Theory and Application of Mathieu Functions* (Clarendon, Oxford, 1951).

[41] R. A. Ibrahim, *Liquid Sloshing Dynamics: Theory and Applications* (Cambridge University Press, Cambridge, 2005).

[42] S. Ciliberto and J. P. Gollub, Phys. Rev. Lett. **52**, 922 (1984).